Nanoscale

COMMUNICATION

View Article Online
View Journal | View Issue

Cite this: *Nanoscale*, 2016, **8**, 8486

Received 17th December 2015,
Accepted 29th March 2016

DOI: 10.1039/c5nr08980h

www.rsc.org/nanoscale

Tunable and amplified Raman gold nanoprobes for effective tracking (TARGET): *in vivo* sensing and imaging†

Naveen Gandra,[a] Hansford C. Hendargo,[b] Stephen J. Norton,[a] Andrew M. Fales,[a] Gregory M. Palmer[b] and Tuan Vo-Dinh*[a]

We describe the development of a highly tunable, physiologically stable, and ultra-bright Raman probe, named as TARGET (Tunable and Amplified Raman Gold Nanoprobes for Effective Tracking), for *in vitro* and *in vivo* surface-enhanced Raman scattering (SERS) applications. The TARGET structure consists of a gold core inside a larger gold shell with a tunable interstitial gap similar to a "nano-rattle" structure. The combination of galvanic replacement and the seed mediated growth method was employed to load Raman reporter molecules and subsequently close the pores to prevent leaking and degradation of reporters under physiologically extreme conditions. Precise tuning of the core–shell gap width, core size, and shell thickness allows us to modulate the plasmonic effect and achieve a maximum electric-field (E-field) intensity. The interstitial gap of TARGET nanoprobes can be designed to exhibit a plasmon absorption band at 785 nm, which is in resonance with the dye absorption maximum and lies in the "tissue optical window", resulting in ultra-bright SERS signals for *in vivo* studies. The results of *in vivo* measurements of TARGETs in laboratory mice illustrated the usefulness of these nanoprobes for medical sensing and imaging.

Surface-enhanced Raman scattering (SERS) has led to the development of important biomedical analysis and sensing tools ranging from *in vitro* diagnostics to *in vivo* imaging.[1–14] A great challenge for many real-life applications is the development of SERS nanoprobes that are highly stable under harsh physiological conditions often encountered in *in vitro* and *in vivo* measurements.[15] To achieve these critical properties required for biomedical imaging and sensing, several SERS nanoprobes have been previously developed by adsorbing and conjugating Raman reporters on metal nanostructures and doping the Raman reporter in a porous silica shell.[4,16,17] However, in this paper we demonstrate a new Raman nanoprobe that achieves these critical properties while also improving the stability of the reporters *in vivo*-protecting them in a solid shell and preventing any detaching or leaking from occuring in physiological fluids.

Our group has been involved in the development and application of various SERS plasmonic platforms that include nanoparticles, nanopost arrays, nanowires, nanochips, and nanostars.[7–9,18–20] More recently, the concept of trapping Raman reporters between the gold core and gold shell nanostructures has shown significant promise in developing ultra-bright SERS probes.[5,21–23] Specifically, SERS probes having an internal gap between the core and shell structures have demonstrated great potential to produce physiologically stable and ultrabright SERS probes for *in vitro* and *in vivo* applications.[5,21] Different types of designs including DNA, polymer, and 1,4-benzenedithiol (BDT) templated SERS probes with uniform internal gaps have been demonstrated successfully.[21,24] However, most of these previous nano-platforms were limited to a few specific Raman dyes and experience difficulty tuning the gap between the core and shell. Therefore, it is important to develop novel core–shell nanostructures with a tunable core–shell gap that allows for loading multiple Raman reporters, which can be used for multiplexing.

In this work, we have developed a new type of SERS probe, *i.e.* a nanorattle with a tunable gap between the core and shell, which is referred to as Tunable and Amplified Raman Gold Nanoprobes for Effective Tracking (TARGET). This TARGET core–shell nanostructure is comprised of a resonance Raman reporter trapped between the core and shell, which effectively acts as an ultra bright SERS probe as a result of a strong and localized electric field due to plasmonic coupling at core–shell junctions. Unlike previously developed "bilayered Raman intense gold nanostrcutures with hidden tags" (BRIGHTs) in which 1,4-benzenethiol (BDT) is required to form a gap between the core and shell, the TARGET nanoprobes have a tunable core–shell gap that allows loading of any chosen resonance or nonresonance Raman reporter.

[a]*Duke University, Departments of Biomedical Engineering and Chemistry and the Fitzpatrick Institute for Photonics, 2589 CIEMAS, Durham, NC 27708, USA. E-mail: tuan.vodinh@duke.edu; Fax: +1 919-684-4488; Tel: +1 919-660-8520*
[b]*Duke University, Department of Radiation Oncology, 203 Research Dr, Durham, NC 27710, USA. E-mail: greg.palmer@duke.edu; Fax: +1 919-684-8718; Tel: +1 919-613-5053*

†Electronic supplementary information (ESI) available. See DOI: 10.1039/c5nr08980h

The tunability of the SERS signal of the TARGETs is multifactorial and governed by the spectral absorption properties of the reporter, excitation wavelength, extinction of the probe, gap size, and loading capacity of reporter molecules between the core and shell. Indeed, the optical properties of the TARGETs can be highly customized to specific excitation wavelengths by carefully tuning the gap width and choosing the resonance reporter specific to the wavelengths of interest. Recent experimental and theoretical studies show that Raman reporters trapped between the core and shell of plasmonic nanostructures drastically improve the SERS signal intensity by several orders of magnitude compared to conventional nanoprobes.[21,22] The advantages of TARGETs compared to other SERS probes are: (i) a highly tunable gap with a well defined core–shell thickness and interstitial gap desired for wavelength specific E-field enhancement, (ii) an ultrabright SERS signal due to strong plasmonic coupling, (iii) physiologically stable reporters protected inside the gap, (iv) consistant SERS signal, and (v) potential for multiplex sensing.

The synthesis of TARGETs is a multi-step process as illustrated in Fig. 1A, starting with the synthesis of 20 nm gold nanoparticles (AuNP) using a seed mediated growth method with cetyl trimethylammonium chloride (CTAC) as the surfactant (Fig. 1B).[21] 20 nm AuNPs were then used as seed templates to grow a 15 nm thick silver shell (Fig. 1C). The silver shell was further used as a sacrificial template to synthesize porous gold/silver nanocages (Au/Ag nanocage) using the previously reported galvanic replacement process (Fig. 1A).[5,25–27] The production of pores allowed us to load resonance Raman reporter molecules between the core and shell using a phase change material, 1-tetradecanol, a well known gate keeper material successfully employed to load drugs in gold nanocages and gold nanorattles.[5,6,28,29] Subsequently, a 5–15 nm thick gold shell was grown on the top of the Au/Ag nanocage to close the pores and to stop the Raman reporter molecules from leaking out even in physiologically stringent conditions. Recent reports suggest that the Au/Ag nanocages could degrade *in vivo*, which could be a limiting factor for biological use of SERS probes.[15] Our approach, however, not only stops the leaking of the reporter dye molecules but also makes them highly stable under *in vivo* conditions compared to Au/Ag nanocages. Once the resonance Raman reporter molecules are loaded, nanocages were vigorously sonicated (10 min) and centrifuged two times to remove weakly adsorbed dye molecules from the surface of the nanostructures. It is important to note that the sonication temperature should not exceed 37 °C. Then 10 ml of CTAB (cetyl trimethylammonium bromide) (0.1 M) and $HAuCl_4{\cdot}3H_2O$ (4.5 mM) solution was reduced with 1 ml of ascorbic acid (0.1 M). At this stage, the color of the solution turned from pale yellow to colorless, which indicates formation of Au^{1+} from Au^{3+}. 5 ml of centrifuged gold nanocages (1 nM) with resonance Raman reporter was added to the growth solution to form a solid gold shell by successfully trapping resonance reporters between two concentric gold layers with a well defined gap (Fig. 1D).

UV/Vis absorption spectra clearly indicate the change in optical properties when the AuNP (plasmon absorption at 518 nm for nanoparticles) transform to silver-coated AuNP –Ag@AuNP– (plasmon absorption at 400 nm for shell structures) followed by galvanic replacement and shell growth to form TARGET (plasmon absorption at 530 to 550 nm for TARGET) (Fig. 1E). Interestingly, we noticed a shoulder between 600 and 700 nm in the UV/Vis absorption spectrum of TARGETs, which is an indication for the plasmon band associated with the gap structure between the core and shell. This shoulder is more obvious if the gap between the core and shell is larger than 5 nm. Our results are consistant with previously reported nanorattle absorption properties. To estimate the E-field enhancement as a function of wavelength in the gap between the core and shell where the Raman reporters reside, we performed both analytical and finite element method (FEM) calculations using COMSOL Multiphysics v4.3 software. The COMSOL calculations show the maximum E-field is concentrated between the core and shell at 755 nm with 40 nm diameter of TARGET, 1 nm gap between the core and shell, and 10 nm shell thickness (40 nm(10-1-18)). Our simulations are in good agreement with analytical calculations (Fig. 1F). Our simulation results clearly indicate that the Raman reporters between the core and shell exhibit a maximum E-field between 600 and 900 nm depending on the shell thickness, core size, and gap size (Fig. S4†), which is important for both *in vitro* and *in vivo* SERS applications.

As mentioned above, the method we have developed in this work can not only trap the resonance reporter but also tune the gap between two concentric gold layers. To demonstrate tunability of the gap between core and shell experimentally, we performed galvanic replacement, reporter loading, and shell growth using two different sacrificial silver templates (10 and 20 nm). The TEM images in Fig. 2A and B clearly show the variation of the gaps when we used two different sizes of silver templates (10 and 20 nm). UV-vis extinction spectra depict the differences in size and gap of the TARGETs. Depending on the gap and size of TARGET, the extinction maximum varied between 525 nm and 550 nm with a shoulder between 600 and 700 nm. The intensity and position of the shoulder depends on the size of the gap between core and shell (Fig. 1E).

Once we determined the optical properties of TARGETs, we focused our studies on the SERS characteristics of the reporter molecules trapped between the core and shell. We measured the SERS signal of 2-[7-(1,3-dihydro-1,3,3-trimethyl-2*H*-indol-2-ylidene)-1,3,5-heptatrienyl]-1,3,3-trimethyl-3*H*-indolium iodide (HITC) molecules trapped in two different TARGETs with 5 and 10 nm gaps (Fig. 2C). The SERS intensity of HITC from the TARGETs having a 10 nm gap was 4.0 ± 0.5 times higher than those with 5 nm gaps. This could be explained by the presence of larger numbers of HITC molecules in the 10 nm gap. The lower SERS signal from the TARGETs with 5 nm gaps could be due to the trade-off between the E-field enhancement and loading capability. The theoretical loading capacity of the 10 nm gap, 20 nm core TARGET is 8.3×10^{-20} mol per particle, assuming a 10 : 1 weight ratio of tetradecanol : HITC.[6] In another

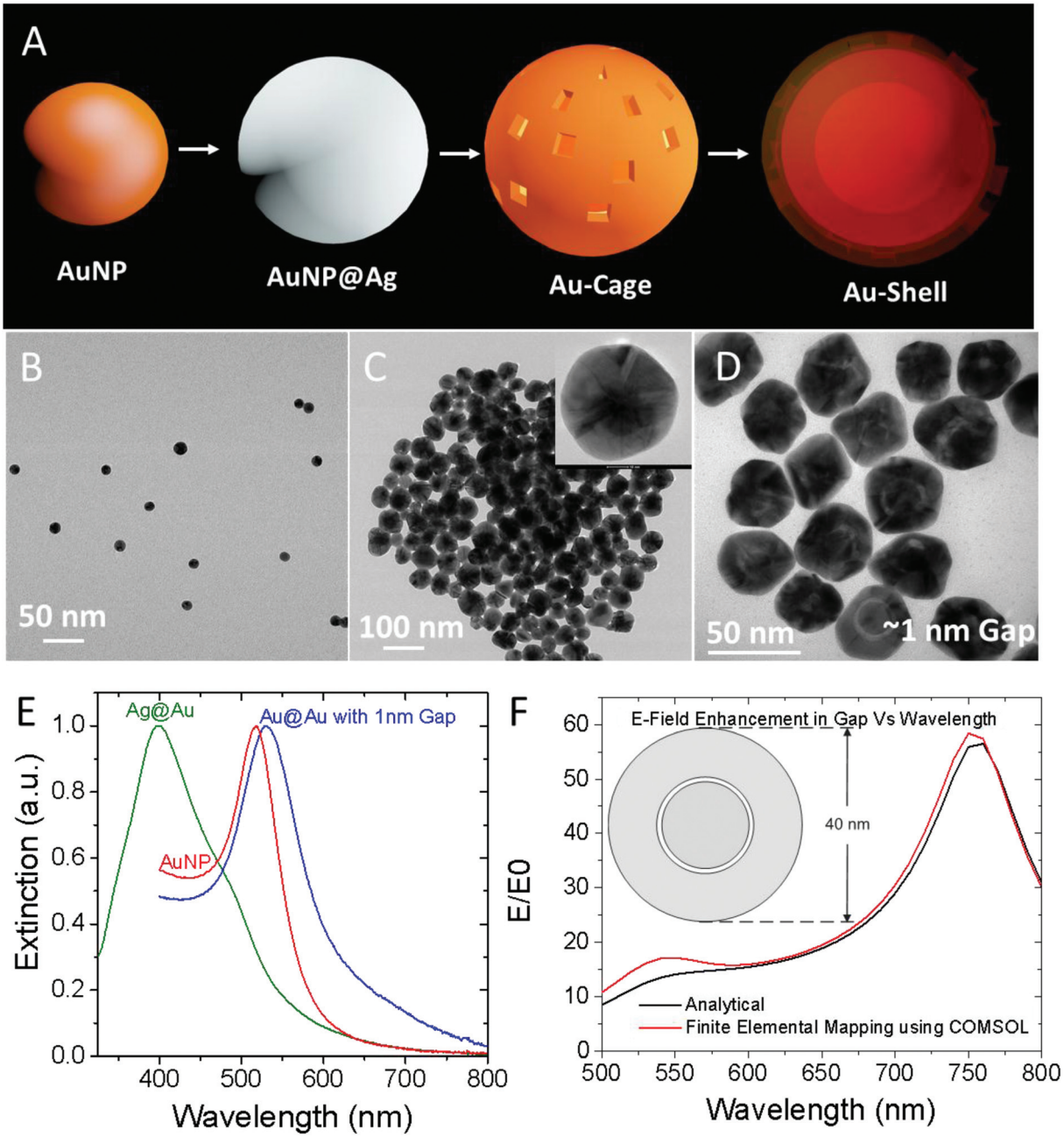

Fig. 1 Design, synthesis, and loading of reporters between gold core and gold shell. (A) Schematic representation of the design and synthesis of core–shell SERS probe with a gap. (B) TEM image of gold core nanoparticles (AuNP) synthesized in Turkevich method (C) TEM image of Ag@AuNP nanostructures with ~20 nm thick silver shell on shell (D) TEM image of core–shell gold-nanoparticle with 2 nm gap between core and shell (E) UV-vis extinction spectra of AuNP, Ag@AuNP, and gold core–shell, which are mentioned above depicting the optical properties of the structures (F) COMSOL model and analytical calculation of the E-field enhancement in the gap at different excitation wavelengths, which predicts 40 nm TARGET nanoparticle with a 1 nm gap has highest E-field at 750 nm. Both analytical and finite elemental mappings are in good agreement with each other.

recent study, we have shown that TARGETs provide 2.40×10^3 higher SERS intensity in comparison to 60 nm gold spheres.[30]

Although such strong Raman enhancement is believed to be from the HITC molecules present between the core and shell of the TARGET structure, and not from dye molecules adsorbed onto the TARGET outer surfaces, we performed etching studies using H_2O_2 in order to study the effect of SERS intensity over time. If the HITC molecules are adsorbed only on the outer surface, the SERS signal is expected to completely diminish in minutes after H_2O_2 etching since the cyanine dyes are known to degrade in peroxide solutions (Fig. S5†). But the SERS intensity was stable up to 2 h after the H_2O_2 addition (Fig. 3C), which confirms that HITC molecules are not on the surface. After 6 h the SERS signal was drastically reduced (Fig. 3), mainly due to the

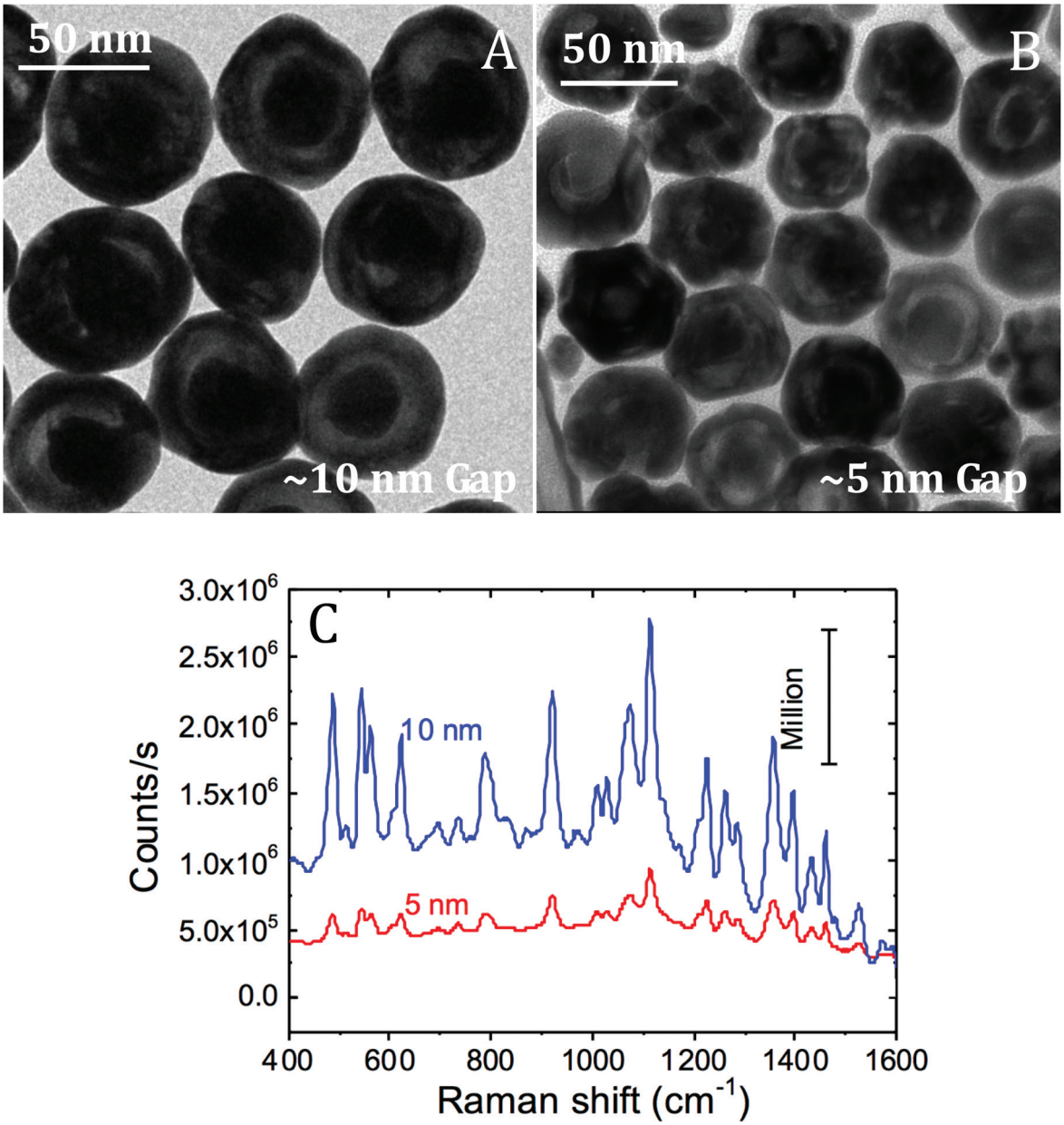

Fig. 2 Tuning the gap between core and shell *versus* SERS. TEM image of HITC molecules trapped in TARGETs with 10 nm (A) and 5 nm (B) gaps between core and shell. (C) SERS of TARGETs with 10 nm and 5 nm gaps.

rupture of the shell, which triggered leaking and degradation of reporter molecules as indicated schematically in Fig. 3C. Our TEM analysis also confirmed the etching and rupture of the shell at 1 and 3 h after H_2O_2 addition (Fig. 3A and B).

Once we confirmed the presence of reporter molecules between the core and shell of a TARGET, as a proof of concept, we further loaded two other Raman reporters Rose Bengal and Methylene Blue for comparative SERS measurements with HITC at 785 nm. The absorption properties of these three dyes are shown in Fig. 4A. After loading these three dyes in three different TARGETs having 10 nm gaps, we achieved maximum SERS intensity in the case of HITC followed by Methylene Blue, but we observed a weak SERS signal for Rose Bengal. In order to achieve maximum SERS it is imperative to have an overlap between the absorption of the resonance reporter, the E-field peak spectrum inside the gap, and excitation wavelength of the laser.

Physiological stability of SERS probes is an important feature for biomedical applications. In our TARGET design, the well-protected reporter molecules inside the core–shell gap are not accessible to physiological fluids and should give consistent SERS signals. This unique feature enables the SERS-encoded core–shell platform to be suitable for use as an internal reference standard. To assess the physiological stability, we incubated TARGETs with breast epithelial cell in culture and collected the SERS signal at different time points

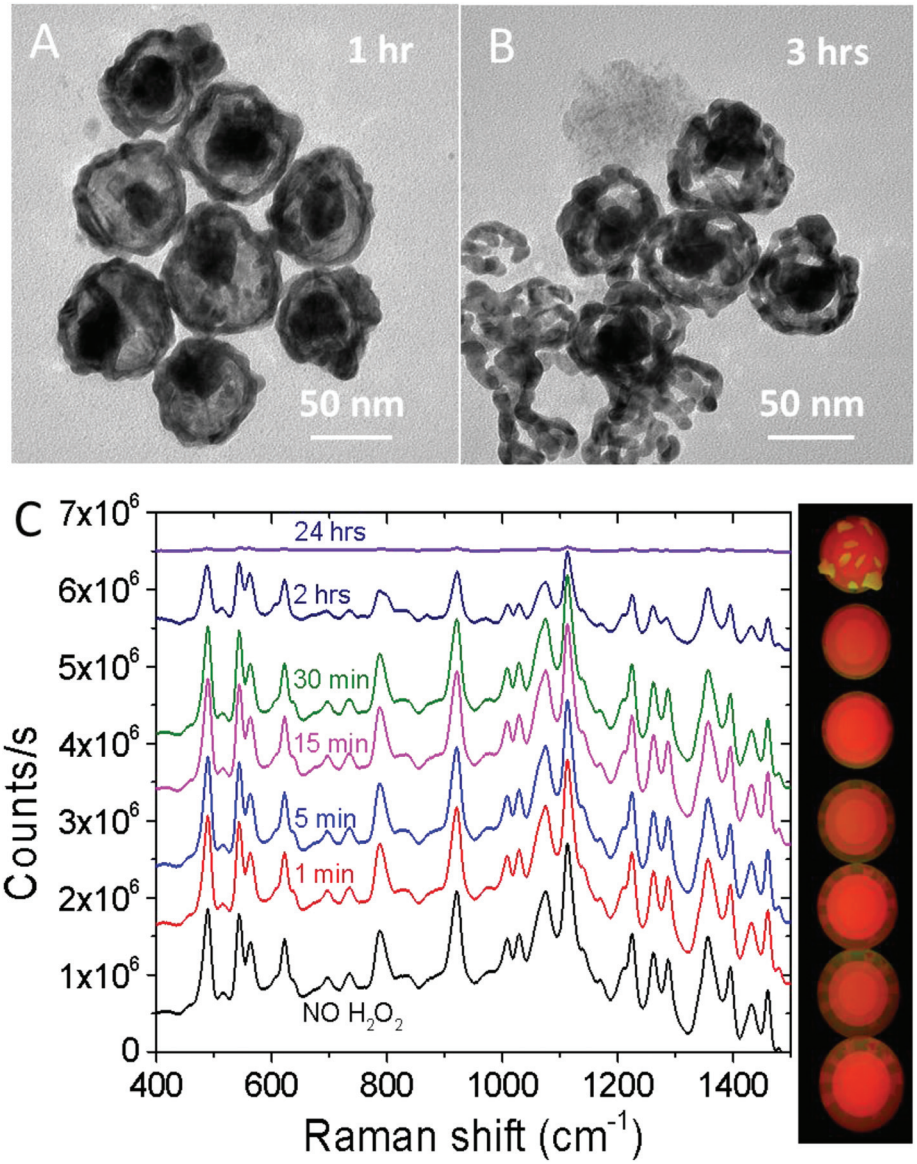

Fig. 3 SERS of HITC present between core and shell with 10 nm gap and 10 nm thick shell in 3% H_2O_2 over time. There is no significant difference in SERS with and without H_2O_2 in first 30 min (as indicated by comparing no H_2O_2, 1 min, 5 min, 15 min, 30 min). But after 24 h intensity of SERS significantly decreased mainly due to the formation of pores, complete etching of shell, and degradation of HITC in peroxide solution.

(Fig. 5A). The color of MCF-10A cells after 5 h of incubation with TARGETs showed a dark color compared to control cells and medium alone (tube 1 in inset, Fig. 5B), which indicated the TARGETs were passively internalized and/or adsorbed on cellular membranes. The intensity of the SERS signal was stable even after 24 h of incubation, which indicated no degradation of either TARGETs or reporter molecules with the cellular system. We performed SERS mapping (Fig. 5B) to confirm the distribution of TARGETs in single MCF-10 A cells. Our SERS mapping results using a 633 nm (10 mW) laser with 1-micron spatial resolution indicated TARGETs were distributed evenly in cellular systems. The SERS imaging data confirmed the stability of the dyes inside TARGETs even after thorough exposure to cellular enzymes.

Furthermore, to study the stability of the TARGET nanoprobes in live animals and tumoregenic conditions, TARGETs were directly injected into the Lewis Lung carcinoma tumor in an athymic immune compromised mouse (commonly known as nude mouse) with a dorsal window chamber and the SERS signal monitored over time (Fig. 5C). The injection site was wiped with an alcohol swab and the SERS signal was collected at a site adjacent to the injection site. SERS signal from TARGETs was collected for 1 s using a fiber optic probe and a 785 nm laser (100 mW) after 15 min, 30 min, 5 h, and 24 h (Fig. 5C) post-injection. Even 24 h after TARGETs injection, the SERS signal was detectable and a decrease in signal intensity was observed between 5 h and 24 h. The drop in SERS intensity was due to the fact that some of the TARGETs entered into the

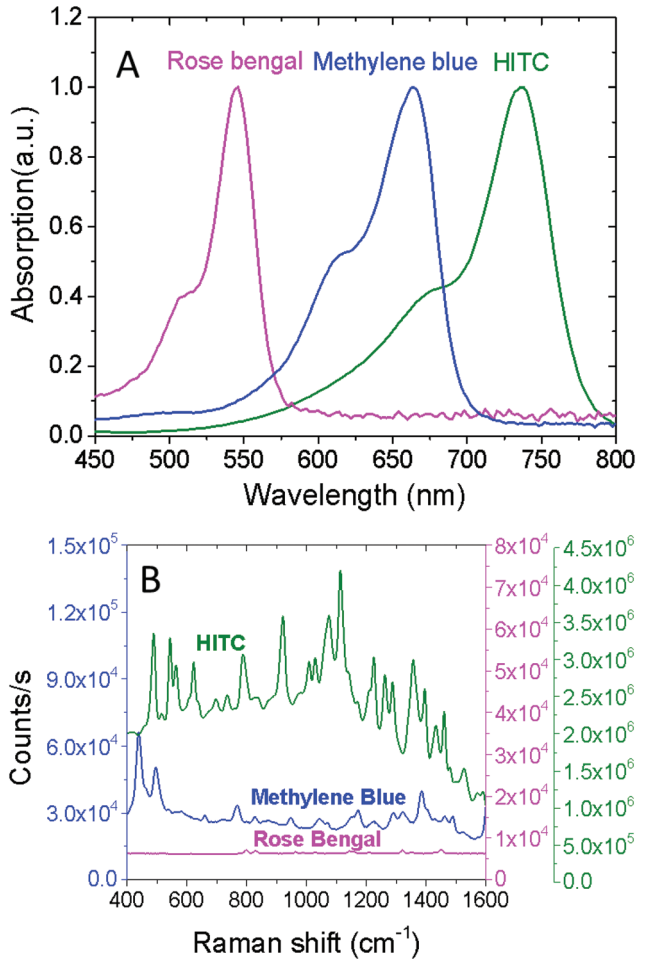

Fig. 4 Loading different reporter molecules (A) absorption spectra of HITC, Methylene Blue, and Rose Bengal (B) SERS of corresponding Raman reporters, HITC shows maximum enhancement (1 million counts per s) followed by methylene blue (40 000 counts per s). But no SERS was observed in the case of Rose Bengal at 785 nm excitation source laser.

blood circulation. We confirm the presence of TARGETs non-invasively in spleen or liver by collecting the SERS signal from different locations along the ventral side of the animal. These results clearly indicate that the TARGETs are highly stable to tissue foreign body response and tumor-associated enzymes.

Finally, we tested the TARGET probes to track their location *in vivo* after intravenous injection in a transgenic CX3CR1-EGFP/FLK1-mCherry mouse with an intact immune system. Stability of the probes after circulation in the bloodstream is extremely important for targeted delivery and for potential use as contrast agents and/or sensing probes. To confirm the accumulation of SERS probes in the tumor present in a window chamber (Fig. 6B), we performed two photon luminescence (TPL) of TARGETs in the live mouse prior to the SERS measurements (Fig. 6C and S6†). After 24 h of *in vivo* circulation in the immune competent mouse, the animal organs were harvested and the SERS signals were measured from the harvested tumor, kidney, heart, spleen, liver, and skin. No detectable SERS signal was found in the blood, which indicates the TARGETs were eliminated from the blood circulation and accumulated in the spleen and tumor after 24 h.

In conclusion, we have developed a novel method to synthesize an ultrabright and physiologically stable SERS probe with a tunable gap for noninvasive *in vivo* tracking and imaging. The proof of concept *in vivo* SERS studies were performed in both immune compromised and immune competent mice, which shows that the TARGETs could be used as potential probes for long-term *in vivo* sensing and imaging applications.

Experimental

Synthesis of porous nanorattles

A silver shell was grown around the gold nanostructures (18 nm) (AuNP), which subsequently transformed into a porous gold shell using galvanic replacement reaction. To grow the silver shell on AuNP, polyvinylpyrrolidone (PVP) was employed as the stabilizing agent. Silver nitrate ($AgNO_3$) solution (5 mM) was added to the above mixture and stirred vigorously for 10 s. The reaction solution was left undisturbed for 2–3 days to allow the formation of Ag@AuNP nanostructures at room temperature. The size of the silver shell was adjusted by changing the amount of precursor AuNPs seeds or by changing amount of $AgNO_3$ solution. Galvanic replacement reaction was employed to transform the silver shell on AuNP into a porous gold shell. The Ag@AuNP solution was centrifuged for 10 min at 8000 rpm and suspended in 1 mM PVP solution. The PVP-modified Ag@AuNP solution was brought to boil by heating to 100 °C. $HAuCl_4$ (1 mM) solution was added to the Ag@AuNPs, while the solution was constantly stirred. Addition of gold salt was stopped once the solution turned a vibrant blue/purple color.

Synthesis of cage like nanorattles and loading reporter molecules

The porous nanorattles obtained was centrifuged two times at 8000 rpm and redispersed in a mixture of 2-[7-(1,3-dihydro-1,3,3-trimethyl-2*H*-indol-2-ylidene)-1,3,5-heptatrienyl]-1,3,3-trimethyl-3*H*-indolium iodide (HITC) (or Methylene Blue/Rose Bengal) (0.1 mM) and 1-tetradecanol (10 mg) in 200 μl of ethanol at ~100 °C (molecular and space filling structures are in Fig. S1†). The reaction was allowed to proceed for 1 h to evaporate most of the ethanol and dispersed in ice-cold water to solidify the reporter dye inside the porous nanorattle. The solidified 1-tetradeconol at low temperature (4 °C) was slowly separated from nanorattles in water using 1 ml pipette. Then the nanorattle solution was centrifuged 3–5 times to completely remove the trace HITC molecules. The detailed procedure to load dyes and drugs is available in previous reports.[6,28,29]

Synthesis of nanorattles with gold shell

To form the gold shell on nanorattles loaded with resonance Raman reporters, we used a seed-mediated growth method.

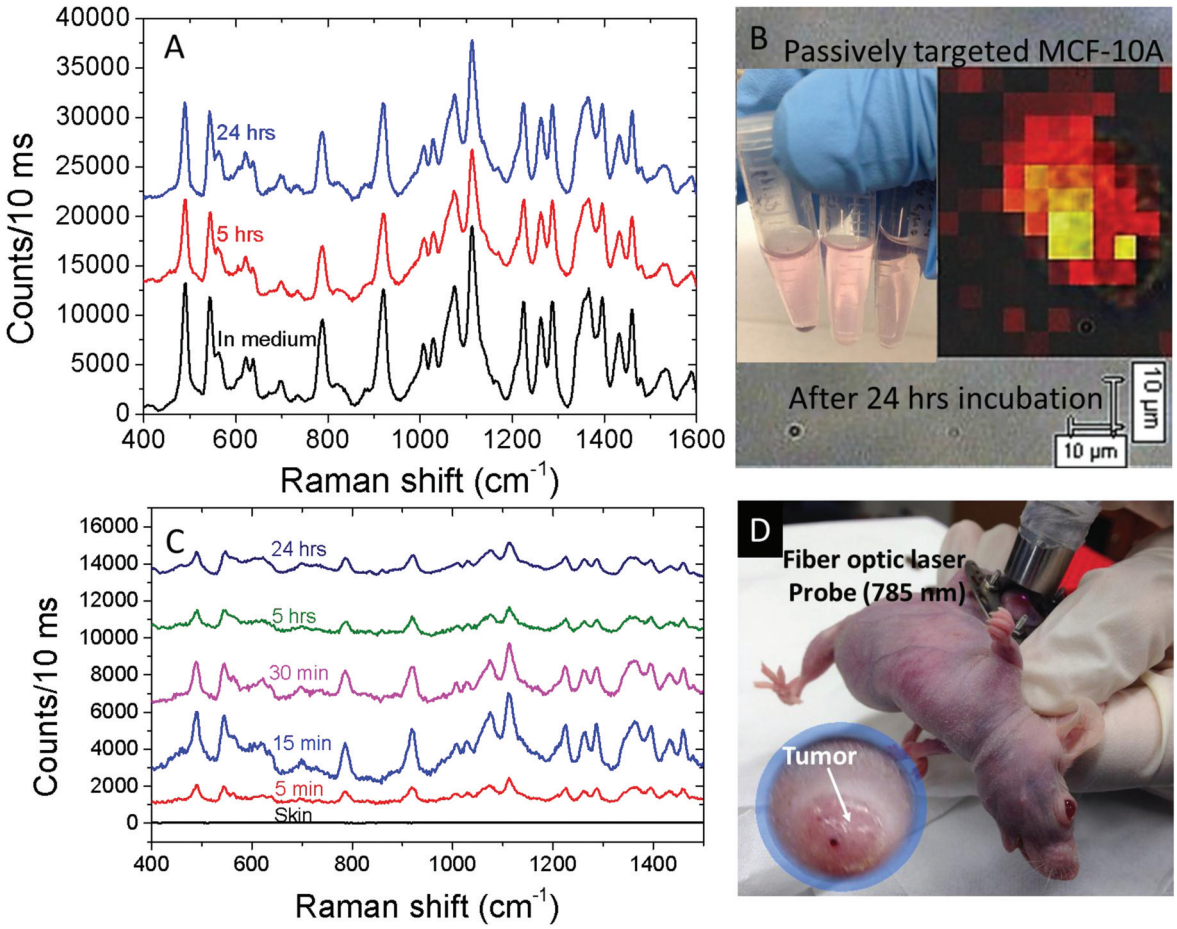

Fig. 5 *In vitro* and *in vivo* stability of SERS probes. (A) *In vitro* stability of SERS probes in passively targeted breast epithelial cells (MCF 10A). SERS of HITC present in the nanoprobes is highly stable even after 5 h and 24 h incubation, which indicates these probes are resistant to cellular enzymatic degradation. (B) *In vitro* SERS mapping of nanoprobes at single cell level to confirm the successful internalization after passive targeting (C) *In vivo* SERS stability of the same nanoprobes in immune compromised mouse with tumor located in window chamber. TARGET nanoprobes were injected directly into the tumor and the SERS signal was followed over time at the injection site. SERS signal from the nanoprobes is detectable even after 24 h following injection at the tumor site, which indicates these probes are not susceptible to tissue response and tumorigenic enzymes. (D) Immune compromised mouse (nude mouse) with tumor located in window chamber; a fiber optic probe was used to excite (785 nm, 100 mW power) and the SERS signal was collected at the tumor location.

Briefly, a gold shell on nanorattles was synthesized using 10 ml of growth solution containing 4.5 mM $HAuCl_4$ and 1 ml of 0.1 M ascorbic acid. Then 1 ml of 1 nM porous nanorattles loaded with reporter molecules were added to the above growth solution and stirred vigorously for 10 s. The reaction mixture was let undisturbed (overnight) to form a uniform solid shell. The formation of this shell was confirmed by both TEM and UV/Vis analysis.

In vivo procedures

Mouse window chamber surgeries were performed as described in a reported protocol.[31] Briefly, nude mice were anesthetized with a 100 mg kg^{-1} and 10 mg kg^{-1}, ketamine/xylazine mixture by an intraperitoneal injection and underwent surgery for placement of a dorsal skin window chamber using sterile surgical procedures. A 12 mm diameter flap of skin was dissected away from the front surface of the dorsal skin flap, leaving the opposite fascial plane with its associated vasculature intact. Following skin-fold dissection, a pair of titanium window frames were mounted and sutured to the skin flap. 1×10^5 Lewis Lung Carcinoma (LLC) cells were injected into the center of the window region beneath the fascial plane, and a cover glass was placed over the area of incision. All mice received an injection of 0.05 mg per kg buprenorphine subcutaneously following surgery. Mice were imaged 10 days after surgical implantation of the window chamber to allow time for tumor development. The nanoparticle solution (100 µL of 1 nM, concentration was measured in Nanosight Fig. S2†) was administered to the animals *via* tail vein injection. After 24 hours, two-photon imaging was performed on animals anesthetized using a ketamine/xylazine mixture as previously described.[32] Animals were awake and restrained by hand during SERS imaging measurements. Following imaging, mice were euthanized with 0.05 mL of euthasol (sodium pentobarbi-

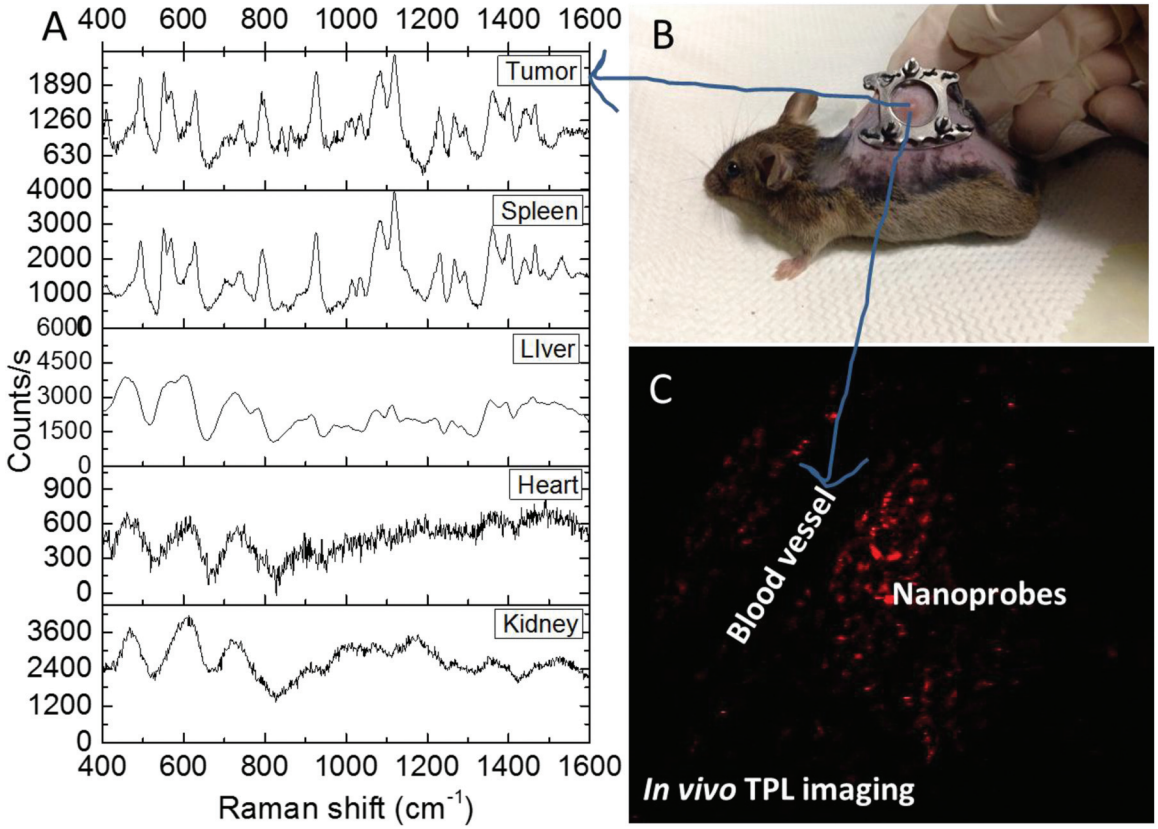

Fig. 6 *In vivo* sensing and imaging. (A) SERS signals of intravenously injected nanoprobes in immune competent mouse after 24 h. Strong SERS signals were detected in both tumor and spleen, which indicated our SERS probes were not affected by the immune competent mouse. (B) Immune responsive mouse with Lewis Lung Carcinoma (LLC) tumor in a dorsal window chamber. (C) *In vivo* two photon luminescence of TARGETs obtained from the tumor location after 24 h of circulation, which indicates that TARGETs accumulated in the tumor due to its leaky vasculature.

tal 390 mg ml^{-1} with sodium phenytoin 50 mg ml^{-1}). Tumor, skin sample, liver, spleen, heart, and kidneys were immediately harvested and placed on ice. All animal procedures were carried out with approval from the Institutional Animal Care and Use Committee (IACUC) at Duke University.

Acknowledgements

The authors would like to thank Dr Douglas Weitzel and Dr Yulin Zhao for their technical assistance with the animal procedures. This work was sponsored by the Defense Advanced Research Projects Agency (HR0011-13-2-0003) and the Duke Faculty Exploratory Fund. The content of the information does not necessarily reflect the position or the policy of the Government, and no official endorsement should be inferred.

References

1 R. A. Alvarez-Puebla and L. M. Liz-Marzan, *Small*, 2010, **6**, 604–610.
2 J. V. Jokerst, A. J. Cole, D. Van de Sompel and S. S. Gambhir, *ACS Nano*, 2012, **6**, 10366–10377.
3 S. Keren, C. Zavaleta, Z. Cheng, A. de la Zerda, O. Gheysens and S. S. Gambhir, *Proc. Natl. Acad. Sci. U. S. A.*, 2008, **105**, 5844–5849.
4 C. L. Zavaleta, B. R. Smith, I. Walton, W. Doering, G. Davis, B. Shojaei, M. J. Natan and S. S. Gambhir, *Proc. Natl. Acad. Sci. U. S. A.*, 2009, **106**, 13511–13516.
5 N. Gandra, C. Portz and S. Singamaneni, *Adv. Mater.*, 2014, **26**, 424–429.
6 L. Tian, N. Gandra and S. Singamaneni, *ACS Nano*, 2013, **7**, 4252–4260.
7 T. Vo-Dinh, *TrAC, Trends Anal. Chem.*, 1998, **17**, 557–582.
8 T. Vo-Dinh, A. M. Fales, G. D. Griffin, C. G. Khoury, Y. Liu, H. Ngo, S. J. Norton, J. K. Register, H.-N. Wang and H. Yuan, *Nanoscale*, 2013, **5**, 10127–10140.
9 T. Vo-Dinh, M. Y. K. Hiromoto, G. M. Begun and R. L. Moody, *Anal. Chem.*, 1984, **56**, 1667–1670.
10 P. Dey, W. Olds, I. Blakey, K. J. Thurecht, E. L. Izake and P. M. Fredericks, *J. Raman Spectrosc.*, 2013, **44**, 1659–1665.
11 N. Gandra and S. Singamaneni, *Nanomedicine*, 2013, **8**, 317–320.
12 H. Kang, S. Jeong, Y. Park, J. Yim, B.-H. Jun, S. Kyeong, J.-K. Yang, G. Kim, S. Hong, L. P. Lee, J.-H. Kim, H.-Y. Lee, D. H. Jeong and Y.-S. Lee, *Adv. Funct. Mater.*, 2013, **23**, 3719–3727.

13 Z. A. Nima, A. Biswas, I. S. Bayer, F. D. Hardcastle, D. Perry, A. Ghosh, E. Dervishi and A. S. Biris, *Drug Metab. Rev.*, 2014, **46**, 155–175.
14 B. Sharma, K. Ma, M. R. Glucksberg and R. P. Van Duyne, *J. Am. Chem. Soc.*, 2013, **135**, 17290–17293.
15 A. M. Goodman, Y. Cao, C. Urban, O. Neumann, C. Ayala-Orozco, M. W. Knight, A. Joshi, P. Nordlander and N. J. Halas, *ACS Nano*, 2014, **8**, 3222–3231.
16 X. Qian, X.-H. Peng, D. O. Ansari, Q. Yin-Goen, G. Z. Chen, D. M. Shin, L. Yang, A. N. Young, M. D. Wang and S. Nie, *Nat. Biotechnol.*, 2008, **26**, 83–90.
17 A. M. Fales, H. Yuan and T. Vo-Dinh, *J. Phys. Chem. C*, 2014, **118**, 3708–3715.
18 H. Yuan, A. M. Fales, C. G. Khoury, J. Liu and T. Vo-Dinh, *J. Raman Spectrosc.*, 2013, **44**, 234–239.
19 A. M. Fales, H. Yuan and T. Vo-Dinh, *Langmuir*, 2011, **27**, 12186–12190.
20 A. M. Fales, H. Yuan and T. Vo-Dinh, *Mol. Pharm.*, 2013, **10**, 2291–2298.
21 N. Gandra and S. Singamaneni, *Adv. Mater.*, 2013, **25**, 1022–1027.
22 D.-K. Lim, K.-S. Jeon, J.-H. Hwang, H. Kim, S. Kwon, Y. D. Suh and J.-M. Nam, *Nat. Nanotechnol.*, 2011, **6**, 452–460.
23 J. Song, B. Duan, C. Wang, J. Zhou, L. Pu, Z. Fang, P. Wang, T. T. Lim and H. Duan, *J. Am. Chem. Soc.*, 2014, **136**, 6838–6841.
24 B. Y. Zhao, J. Shen, S. Chen, D. Wang, F. Li, S. Mathur, S. Song and C. Fan, *Chem. Sci.*, 2014, **5**(11), 4460–4466.
25 J. Chen, F. Saeki, B. J. Wiley, H. Cang, M. J. Cobb, Z.-Y. Li, L. Au, H. Zhang, M. B. Kimmey, X. Li and Y. Xia, *Nano Lett.*, 2005, **5**, 473–477.
26 S. E. Skrabalak, J. Chen, Y. Sun, X. Lu, L. Au, C. M. Cobley and Y. Xia, *Acc. Chem. Res.*, 2008, **41**, 1587–1595.
27 X. Xia, Y. Wang, A. Ruditskiy and Y. Xia, *Adv. Mater.*, 2013, **25**, 6313–6333.
28 S.-W. Choi, Y. Zhang and Y. Xia, *Angew. Chem., Int. Ed.*, 2010, **49**, 7904–7908.
29 G. D. Moon, S.-W. Choi, X. Cai, W. Li, E. C. Cho, U. Jeong, L. V. Wang and Y. Xia, *J. Am. Chem. Soc.*, 2011, **133**, 4762–4765.
30 H. T. Ngo, N. Gandra, A. M. Fales, S. M. Taylor and T. Vo-Dinh, *Biosens. Bioelectron.*, 2016, **81**, 8–14.
31 G. M. Palmer, A. N. Fontanella, S. Shan, G. Hanna, G. Zhang, C. L. Fraser and M. W. Dewhirst, *Nat. Protocols*, 2011, **6**, 1355–1366.
32 H. Yuan, C. G. Khoury, H. Hwang, C. M. Wilson, G. A. Grant and T. Vo-Dinh, *Nanotechnology*, 2012, **23**, 075102.